minerals

IMPACT FACTOR 2.2

CITESCORE 4.4

Article

# New Contributions to Mineralogical and Geochemical Knowledge of Old Preguiça Mine, Beja, Portugal

Teresa P. Silva, Igor Morais, Sofia Soares, Ivo Rodrigues, Daniel P. S. de Oliveira and José Mirão

Special Issue

Mineralogical and Geochemical Characterization of Geological Materials, 2nd Edition

Edited by

Dr. Teresa Pereira da Silva, Dr. Daniel P. S. De Oliveira and Dr. João Pedro Veiga

MDPI

https://doi.org/10.3390/min16040348

*minerals*

MDPI

*Article*

# New Contributions to Mineralogical and Geochemical Knowledge of Old Preguiça Mine, Beja, Portugal

**Teresa P. Silva [1,*], Igor Morais [2], Sofia Soares [3], Ivo Rodrigues [4], Daniel P. S. de Oliveira [1,5] and José Mirão [6,7]**

1 LNEG (National Laboratory for Energy and Geology), Mineral Resources and Geophysics Research Unit, Estrada da Portela, Apartado 7586, 2610-999 Amadora, Portugal; daniel.oliveira@lneg.pt
2 LNEG (National Laboratory for Energy and Geology), Mineral Resources and Geophysics Research Unit, Bairro de Val d'Oca, Apartado 14, 7601-909 Aljustrel, Portugal; igor.morais@lneg.pt
3 LNEG (National Laboratory for Energy and Geology), Geology, Hydrogeology and Coastal Geology Research Unit, Estrada da Portela, Apartado 7586, 2610-999 Amadora, Portugal; sofia.soares@lneg.pt
4 Rua D. Afonso III, n.º 22 D, 7800-050 Beja, Portugal; ivombrodrigues@gmail.com
5 Mineral Resources Expert Group, EuroGeoSurveys, Rue Joseph II, 36–38, 1000 Brussels, Belgium
6 Laboratório Hércules, Universidade de Évora, Largo Marquês de Marialva 8, 7000-809 Évora, Portugal; jmirao@uevora.pt
7 Laboratório Associado In2Past, Universidade de Évora, Largo Marquês de Marialva 8, 7000-809 Évora, Portugal
* Correspondence: teresa.pena@lneg.pt

## Abstract

Abandoned mining areas provide valuable opportunities to investigate ore-forming processes, supergene mineral transformations, and the geochemical behaviour of metals. In this sense, the old Preguiça mine (Beja, Portugal), exploited for Fe–Zn–Pb, was studied providing new mineralogical and geochemical data aimed at improving the understanding of the secondary mineral assemblages of this deposit. A total of 70 samples collected from three accessible underground levels (first, second and third) and mine waste, complemented by 16 samples from a deeper level (fourth) previously collected, were analysed using X-ray diffraction (XRD), scanning electron microscopy (SEM), and a portable X-ray fluorescence (pXRF) equipment. Mineralogical phases are dominated by a wide range of secondary oxides, carbonates, arsenates, vanadates, silicates, phosphates and sulphates, but remnants of primary sulphides were also found. The following minerals can be emphasised: goethite, hematite, calcite, dolomite, descloizite, willemite, mimetite, cerussite, smithsonite and fraipontite. The presence of massicot in the Preguiça mine, is described for the first time. Bulk geochemical analyses show high concentrations of Fe, Ca, Zn and Pb, consistent with the observed mineralogy. The presence of vanadium- and arsenic-bearing minerals highlights the occurrence of critical raw materials, supporting the importance of reassessing other abandoned mining areas in the context of sustainable resource management and strategic raw-material planning.

**Keywords:** Preguiça mine; mineral phases; pXRF; historical Fe–Zn–Pb deposit; abandoned mine; Portugal



Academic Editor: Alexander Mikhailovich Kalinkin

Received: 11 February 2026
Revised: 23 March 2026
Accepted: 24 March 2026
Published: 26 March 2026



## 1. Introduction

Within the European Union, historical mining districts are increasingly recognised as potential contributors to resource security strategies, aligning geological research with circular economy and resource efficiency policies.

Additionally, abandoned mining areas provide valuable natural laboratories for investigating ore-forming processes, mineral transformations, and the geochemical behaviour of metals in supergene environments. The weathering of primary ore minerals and subsequent supergene processes can generate complex assemblages of secondary phases that evidence important information about fluid–rock interaction, element mobility, and post-depositional alteration [1]. Earlier exploration and analytical approaches—designed primarily to target the metals of interest at the time—now offer valuable opportunities for reassessment. By applying innovative methodologies and advanced analytical techniques, these areas can be re-examined for additional elements of interest. Advances in mineralogical characterisation techniques, have facilitated the identification of trace-element hosts and previously overlooked mineral species, thereby providing new insights into metal distribution and enrichment processes. The re-examination of abandoned mining areas represents an important approach for assessing secondary resources that may contribute to the future supply of critical and strategic raw materials (CRM and SRM) [2,3].

The old Preguiça mine (Moura, Beja, Portugal), located in the Ossa Morena Zone (OMZ), is an emblematic site within the context of Portugal's extensive mining heritage and holds a significant place in the region's mining history [4]. Preguiça constitutes a representative example of an abandoned Fe–Zn–Pb mineralisation. Currently, primary sulphide minerals, pyrite, marcasite, chalcopyrite, sphalerite, and galena, are locally preserved and occur only sporadically within the mineralized zones. Subsequent weathering has significantly modified the primary mineralisation, producing a diverse suite of secondary minerals including oxides, carbonates, arsenates, vanadates, silicates, and sulphates. These transformations provide important clues on the geochemical mobility of metals such as Zn, Pb, Fe, V and As in oxidising environments, e.g., [5]. Understanding these processes is essential not only for reconstructing the post-mineralization evolution of the deposit but also for evaluating potential environmental risks and resource opportunities associated with secondary mineral phases.

The present work aims to provide new mineralogical and geochemical contributions to the understanding of the Preguiça mine's geological evolution. Through the study of samples collected from four underground levels and mine waste areas, this research seeks to identify the mineral phases present and evaluate the distribution of elements associated with the deposit. By combining X-ray diffraction (XRD), portable X-ray fluorescence (pXRF), and scanning electron microscopy (SEM) techniques, the study contributes to enriching the knowledge of the mineralogical diversity, describing the phase morphology and evaluating the geochemical characteristics of the Preguiça deposit. Furthermore, the results help clarify the role of supergene processes in the formation of secondary mineral assemblages and highlight the potential occurrence of elements of strategic importance within this historical mining environment.

### *1.1. Geological Setting*

The old Preguiça mine is located in southern Portugal, approximately 20 km southeast of the town of Moura. Geologically, the area is located within the Ossa Morena Zone (OMZ), a heterogeneous and complex tectonostratigraphic zone, characterised by distinctive stratigraphic, magmatic and tectono-metamorphic features. These reflect the influence of two successive Wilson Cycles, namely, the Cadomian and Variscan Cycles [6,7], and part of the Magnetitic–Zinciferous Belt or Montemor-o-Novo—Ficalho Belt, where there are known mineralisations of (1) massive magnetite ores; (2) massive and stratiform sulphides ores; (3) iron skarns; (4) Au-As veins and (5) hydrothermal veins containing Cu [8]. The combination of volcanic influences, supergene alteration, Cambrian carbonate host rocks,

two major tectonic overprints, and the resulting mineral–textural transformations make Preguiça a notable geological case.

Geologically, the mine area is dominated by rocks of the Dolomitic Formation with probable Lower Cambrian age (Figure 1), composed at its base of intermediate to basic volcanic rocks and, more rarely with felsic volcanism overlain by dolomitic limestones with approximately 400 m thickness [9–12]. The dolomitic limestones are composed mainly of carbonate assemblages (calcite, dolomite, and ankerite) and accessorily by quartz, muscovite, chlorite, epidote and actinolite–tremolite [13].

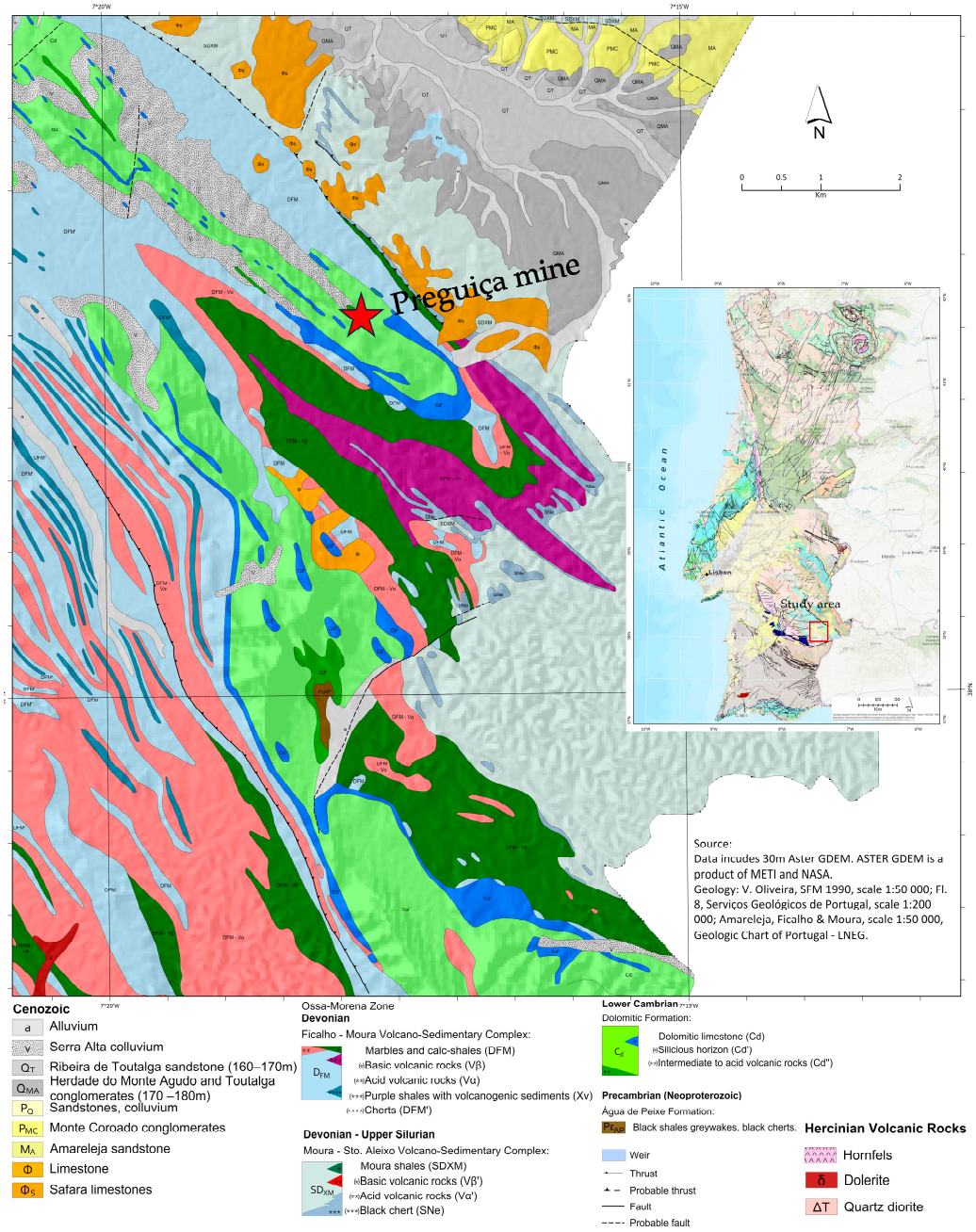


**Figure 1.** Geological map of the Ossa Morena Zone with the location of the Preguiça mine (adapted from [6,14]).

Two ore bodies are recognised from the surface down to the water table (100 m deep), where the primary sulphide mineralisation is found [10,15]. The sulphides' oxidation in the surface produced a gossan zone with 40 m thickness, very enriched in zinc, which was the

major target of exploration in the past (Figures 2 and 3A). In the NE flank of the structure, exploration boreholes crossed the mineralised horizon with 20.4% Zn, 5.2% Pb and 107 ppm of Ag [9,16]. The mineral potential of this area led to further detailed exploration by the former SFM Government Agency (Serviço de Fomento Mineiro, currently LNEG) in the 1980s, as well as several private exploration companies. These surveys generated a large knowledge database containing geologic, soil geochemistry (Cu, Zn, Pb), gravity (Bouguer 2.65) and magnetic (vertical field) data (200 × 200 m grid surveys) [14]. General aspects of the old Preguiça mine can be seen in Figure 3.

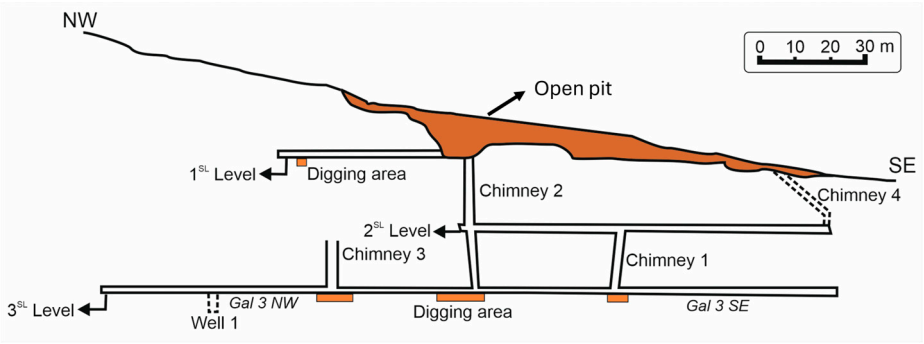


**Figure 2.** General map of the galleries of the old Preguiça mine aligned NW-SE (adapted from [17]).

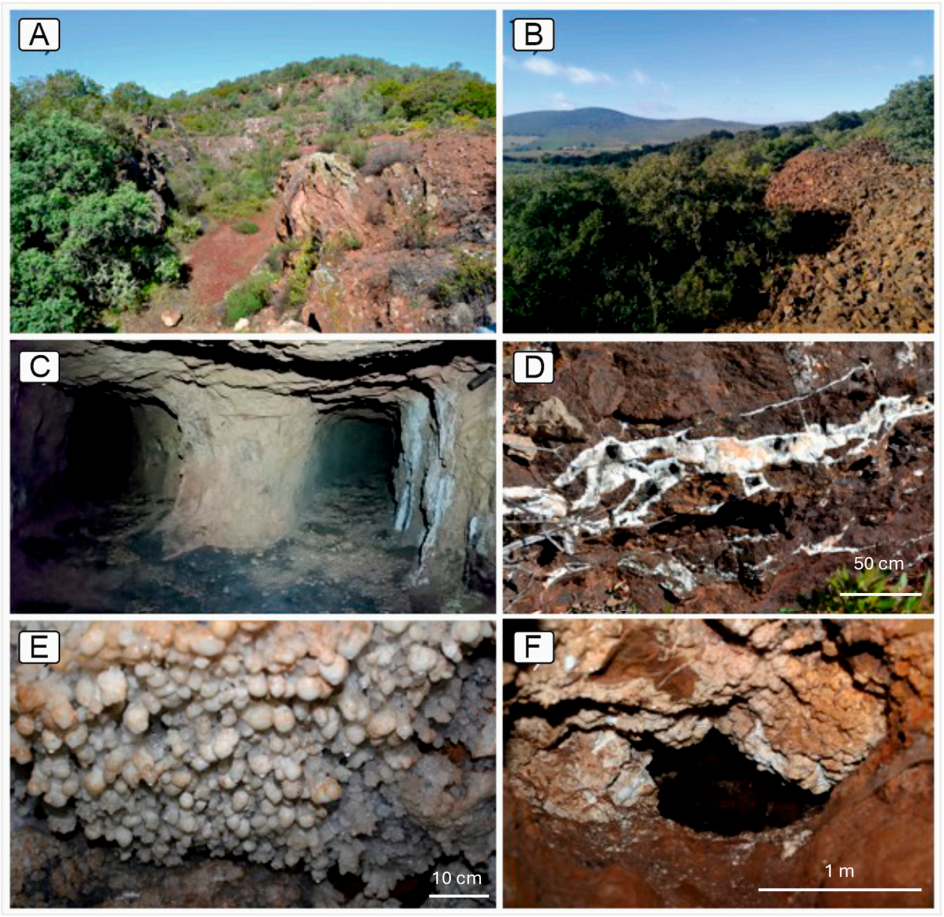


**Figure 3.** General aspects of the old Preguiça mine. (**A**) Open pit area of the gossan zone. (**B**) Mine waste area. (**C**) Ore access galleries on the third level. (**D**) Dolomites of the Dolomitic Formation (Lower Cambrian age) with secondary carbonate veins. (**E**,**F**) Natural cavity with carbonate concretions.

The ore genesis model remains controversial and has been described as comparable to Irish-type sedimentary exhalative (SEDEX) deposits [8,9]. Other authors attribute the primary genesis of the deposits to volcanic-hosted massive sulphide (VHMS) mineralisation, consisting of stratiform massive sulphides hosted in metacarbonate and metavolcanic horizons and affected by intense, albeit heterogeneous, hydrothermal alteration [18].

### *1.2. Historical Mine Overview*

The Moura region has had a long history of mining, possibly from pre-Bronze Age times to the twentieth century [19]. Documented mining concessions in the Preguiça area date back to the late nineteenth century, notably Umbria da Preguiça (Fe–Pb, 1899) and Preguiça No. 6 (Fe–Mn, 1914; originally registered in 1872) [20,21]. Between 1911 and 1915, Preguiça No. 2 was actively exploited, producing approximately 2342 t of ore with grades up to 25% Zn.

Mining ceased due to World War I events and was definitively abandoned in 1929. In the 1950s, the Serviço de Fomento Mineiro (SFM) reassessed the deposits through underground development and sampling, recording Zn contents of up to 31% at the third level of Preguiça No. 2 [17]. This work led to renewed exploitation of the mine by the Compagnie Royale Asturienne des Mines, which acquired the mines in 1960 and resumed mining operations at Preguiça No. 2 under a pilot exploitation regime. New surveys enabled the identification of three mineralized bodies, with total reserves estimated at 600,000 t to 1 Mt, containing 8% Zn and 2% Pb. Mining activity was abandoned in 1966 [9,10]. More recent exploration campaigns were carried out by mining companies APAC (Asia–Pacific) Resources Company (1998), Northern Lion Gold (2007–2009), and Green Arrow/WalZinc (2016–2021), resulting in updated geological mapping and a 3D deposit model. The concession expired in March 2022, and the mine is currently inactive under environmental protection.

## 2. Materials and Methods

### *2.1. Sampling*

A total of 70 samples were collected on the 1st, 2nd and 3rd levels of the mine and at the mine waste open pit, near the 2nd level. Due to the difficulty of accessing the 4th level, 16 samples previously collected by one of the authors (I.R.) were used for this study. Considering the safety conditions, only the 3rd level was adequate for careful sampling around almost all the galleries. Table 1 lists the provenience of each sample.

**Table 1.** Collected samples and their reference positions.

| | 1st Level | 2nd Level | 3rd Level | 4th Level | Open Pit |
|---|---|---|---|---|---|
| Sample Reference | From PR68 to PR70 | PR65 | From PR1 to PR63 | From P4–1 to P4–16 | PR66 |

### *2.2. Methodology*

Small fragments were selected (almost 300) for X-ray diffraction (XRD), using the stereomicroscope (Stemi SV-11, Zeiss, Oberkochen, Baden-Württemberg, Germany), with several images collected using a digital Zeiss camera (Axio-Cam Mrc, Oberkochen, Baden-Württemberg, Germany). To obtain high-quality images of the small crystals, several photographs were taken of the same fragment at different focus planes and then photo-stacked using the programme *Photopea* (https://www.photopea.com/, accessed on 23 March 2026).

Powder X-ray diffraction (XRD) data were collected using a D8 Advance Bruker AXS diffractometer (Bruker AXS GmbH, Karlsruhe, Germany) with Cu Kα radiation, operating at 40 kV and 40 mA. The powder diffractograms (5–70° 2θ) were obtained using a step size

of 0.015° and a step time of 0.3 s with a LYNXEYE XE-T detector. XRD data treatment was performed using DIFFRAC.EVA v5.1 software and the Crystallography Open Database (COD) or the Powder Diffraction File database (PDF-2) for phase identification.

Chemical analysis was necessary in some fragments to help phase identification, due to the overlap of some peaks in the XRD spectra and to the solid solution between end members of some mineral groups. For that, a portable X-ray fluorescence (pXRF) equipment, X-MET8000 Expert Geo from HITACHI (Tokyo, Japan), was used in the laboratory using a benchtop stand and the analytical programme "Mining" (60 s per sample), to analyse powder fragments. This apparatus was equipped with a Rh tube (4 W; 50 kV maximum, 200 μA maximum) and a high-resolution silicon drift detector (SDD); the measurement spot size was 10.7 mm × 9.4 mm. pXRF equipment was also used for a bulk chemical analysis, allowing a rapid evaluation of the contents of a wide range of elements. For that purpose, samples were analysed as collected, using the programme "Mining" (for elements with an atomic number higher than Mg) and "REE" (for the rare-earth elements: La, Ce, Pr and Nd, during 180 s). The measurements were acquired by using the internal calibration set up in the equipment as provided by the manufacturer, based on the Fundamental Parameters (FP) method [22,23]. The general details of the equipment's operating mode are described in, e.g., [24].

Some samples were also morphologically and chemically studied through scanning electron microscopy with energy-dispersive spectroscopy (SEM-EDS) in backscattering mode (BSE), providing elemental distribution maps, using a Hitachi™ S-3700N variable pressure SEM (Hitachi, Tokyo, Japan), equipped with a Bruker™ XFlash 5010 silicon drift EDS detector (Bruker Corporation, Berlin, BE, Germany) (resolution: 126 eV at FWHM/Mn Kα). Analyses were conducted at an accelerating voltage of 20 kV, beam current of 120 μA, 10 mm working distance, and a variable pressure mode at 40 Pa, without preparation or carbon coating. Data acquisition and interpretation were carried out using Esprit 1.9 software (Bruker, Berlin, BE, Germany).

## 3. Results and Discussion

### *3.1. Identification of Mineral Species*

The mineralogical phases identified in the Preguiça mine fragments are listed in Table 2. They are in accordance with the findings of other authors in this mine [25–29] or in similar geologic environments [30,31]. The number of occurrences of each phase at each level gives an approximation of their abundance in the total number of fragments analysed (n). Remaining primary sulphides (pyrite, marcasite, chalcopyrite, sphalerite, and galena), as referred by Gomes et al. [17], were sporadically observed on the third level (Figure 4A,B). Only at this level a magnesium sulphate hydrate (epsomite) was also found, which occurs as a whitish efflorescence (Figure 4C,D) over dolomite. Other secondary minerals, formed in a strongly oxidising environment [25,29], were observed: oxides (Mn, Fe and Pb) and carbonates (Mg, Ca, Fe, Zn and Pb) are spread along the mine, but goethite and quartz are frequent on the fourth level and in the mine waste open pit, while on the third level calcite, goethite and quartz are very frequent, followed by hematite, dolomite and descloizite (vanadate of lead and zinc). The zinc silicate willemite is very frequent on the first level, followed by goethite, quartz and mimetite (lead arsenate), while willemite, hematite and cerussite (lead carbonate) are also frequent in the mine waste open pit. The main mineral species identified are described below through their mineral groups (including illustrative images). Figure 5 displays some examples of the XRD spectra obtained, showing usually a mixture of phases, labelled in the legend of each spectrum.

**Table 2.** Minerals identified on the four levels of the Preguiça mine and in the mine waste open pit. The number of fragments where each mineral was found is displayed (in a total of n fragments analysed); the chlorites and micas formulas are not given (-) for simplicity, as they represent two groups of related mineral species displaying a similar XRD pattern inside each group.

| Mineral Name | Formula | First Level (n = 19) | Second Level (n = 1) | Third Level (n = 216) | Fourth Level (n = 24) | Open Pit (n = 19) |
|---|---|---|---|---|---|---|
| Ankerite | $Ca(Fe^{2+},Mg)(CO_3)_2$ | | | 2 | | |
| Aragonite | $CaCO_3$ | | 1 | 2 | | 1 |
| Arsendescloizite | $PbZn(AsO_4)(OH)$ | | | 1 | | |
| Beaverite (Zn) | $Pb(Fe^{3+}{}_2Zn)(SO_4)_2(OH)_6$ | | | | 1 | |
| Beudantite | $PbFe_3(AsO_4)(SO_4)(OH)_6$ | | | | 2 | |
| Calcite | $CaCO_3$ | 2 | 1 | 114 | 4 | 2 |
| Cerussite | $PbCO_3$ | 1 | | 5 | | 8 |
| Chabazite-Ca | $(Ca,K_2,Na_2)_2[Al_2Si_4O_{12}]_2 \cdot 12H_2O$ | | | 1 | | |
| Chalcopyrite | $CuFeS_2$ | | | 1 | | |
| Chlorites | - | 1 | 1 | 9 | 1 | |
| Coronadite | $Pb(Mn^{4+}{}_6Mn^{3+}{}_2)O_{16}$ | 1 | | | | |
| Descloizite | $PbZn(VO_4)(OH)$ | | | 52 | 1 | |
| Dolomite | $CaMg(CO_3)_2$ | | 1 | 64 | 4 | 1 |
| Epsomite | $MgSO_4 \cdot 7H_2O$ | | | 4 | | |
| Fraipontite | $(Zn,Al)_3((Si,Al)_2O_5)(OH)_4$ | | | 8 | | 2 |
| Galena | PbS | | | 1 | | |
| Goethite | $\alpha$-$Fe^{3+}O(OH)$ | 7 | | 106 | 20 | 13 |
| Gypsum | $CaSO_4 \cdot 2H_2O$ | | | 8 | 6 | |
| Hedyphane | $Ca_2Pb_3(AsO_4)_3Cl$ | | | 4 | 1 | |
| Hematite | $Fe_2O_3$ | 1 | | 53 | 5 | 7 |
| Jarosite | $KFe^{3+}{}_3(SO_4)_2(OH)_6$ | | | 2 | 2 | |
| Magnetite | $Fe^{2+}Fe^{3+}{}_2O_4$ | | | 2 | | 1 |
| Marcasite | $FeS_2$ | | | 1 | | |
| Massicot | PbO | | | 3 | | |
| Micas | - | | | 23 | 2 | |
| Mimetite | $Pb_5(AsO_4)_3Cl$ | 9 | | 17 | 1 | |
| Minrecordite | $CaZn(CO_3)_2$ | | | 5 | | |
| Montmorillonite | $(Na,Ca)_{0.33}(Al,Mg)_2(Si_4O_{10})(OH)_2 \cdot nH_2O$ | | | 2 | | |
| Mottramite | $PbCu(VO_4)(OH)$ | | | 1 | | |
| Phosphohedyphane | $Ca_2Pb_3(PO_4)_3Cl$ | 1 | | 2 | 1 | |
| Plattnerite | $PbO_2$ | | | 4 | | 4 |
| Plumbojarosite | $Pb_{0.5}Fe^{3+}{}_3(SO_4)_2(OH)_6$ | | | 1 | | |
| Pyrite | $FeS_2$ | | | 1 | | |
| Quartz | $SiO_2$ | 9 | 1 | 122 | 19 | 13 |
| Richterite | $Na(NaCa)Mg_5(Si_8O_{22})(OH)_2$ | | | | 1 | |
| Siderite | $FeCO_3$ | | | 2 | | |
| Smithsonite | $ZnCO_3$ | | | 7 | 4 | 1 |
| Sphalerite | ZnS | | | 3 | | |
| Talc | $Mg_3Si_4O_{10}(OH)_2$ | | | 5 | | |
| Vanadinite | $Pb_5(VO_4)_3Cl$ | 1 | | 1 | | |
| Vermiculite | $Mg_{0.7}(Mg,Fe,Al)_6(Si,Al)_8O_{20}(OH)_4 \cdot 8H_2O$ | | | 3 | | |
| Willemite | $Zn_2SiO_4$ | 18 | | 16 | | 12 |

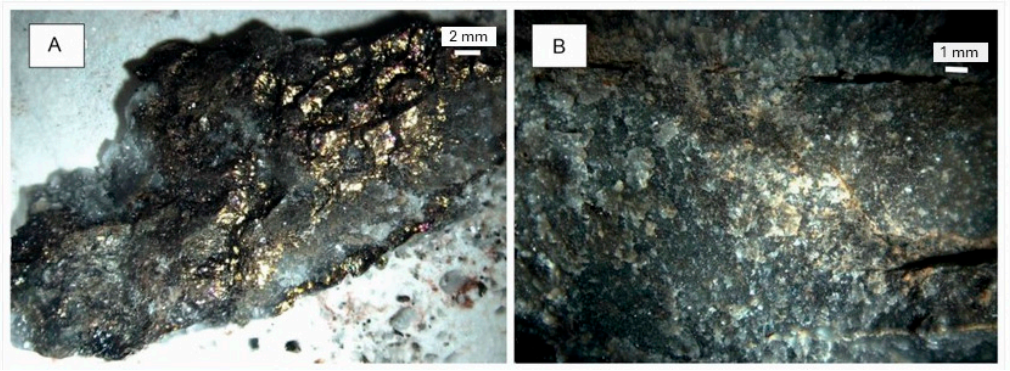


**Figure 4.** *Cont.*

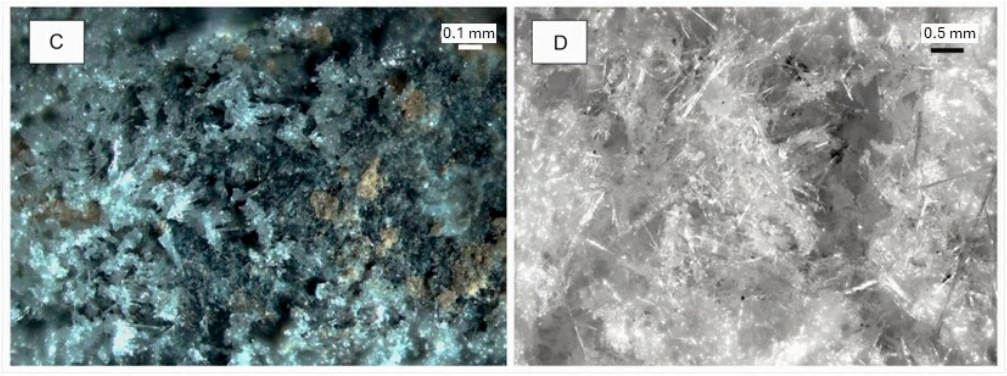


**Figure 4.** Stereomicroscope images of samples collected on the third level of the Preguiça mine. (**A**) Chalcopyrite+sphalerite+marcasite over dolomite (sample PR30). (**B**) Dolomite+pyrite (PR54); (**C**) Epsomite over dolomite (PR29). (**D**) Detail of epsomite crystals.

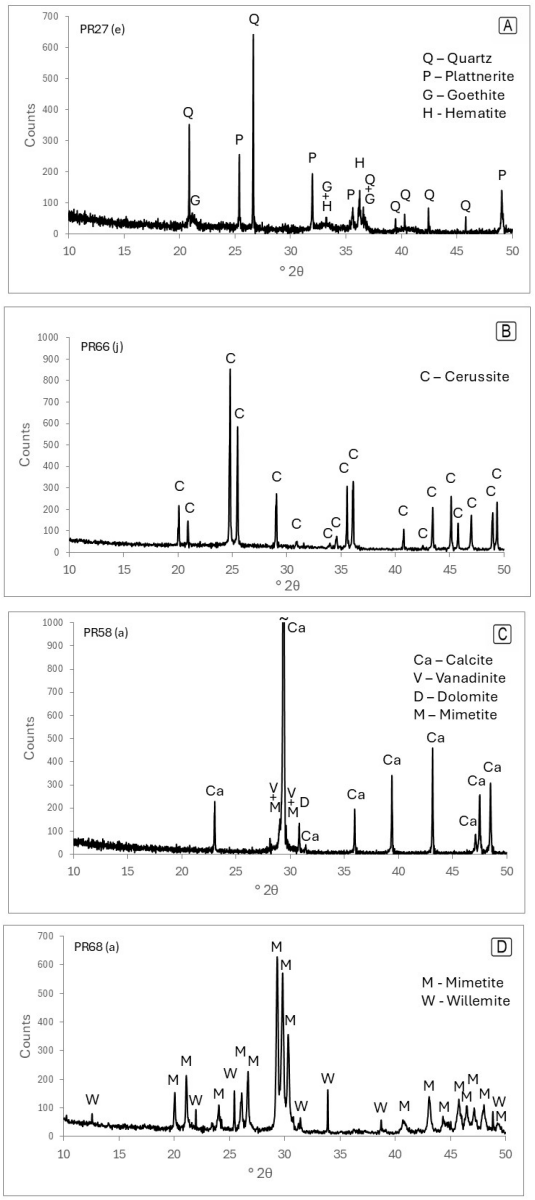


**Figure 5.** Illustrative examples of XRD spectra; the identified phases are shown in the legend: (**A**) sample PR27 (e); (**B**) PR66 (j); (**C**) PR58 (a); (**D**) PR68 (a). The mineral phases are simplified using the first letter/s of their name. COD card numbers: Q—1011172; P—9014175; G—1008766; H—9000139; C—9013803; Ca—9000095; V—9004057; D—9004933; M—1010997; W—9014832.

### 3.1.1. Plattnerite and Massicot

Plattnerite ($PbO_2$), whose XRD pattern is represented in Figure 5A, belongs to the rutile group and has a tetragonal structure. The acicular black crystals were observed on the third level (Figure 6A,B) and mine waste open pit. A BSE image of plattnerite and an example of the EDS spectrum obtained are shown in Figure 6C,D. Overlap between Pb *M* lines and S *K* lines can occur, and therefore the presence of galena cannot be ruled out. Occurrences of plattnerite have been described, e.g., in the Goodsprings mining district of Nevada [32], in Poland [33] and in Leadhills, Scotland [34]. Massicot (PbO), a mineral with orthorhombic structure, whose presence has not yet been described in the Preguiça mine, was sporadically found in traces.

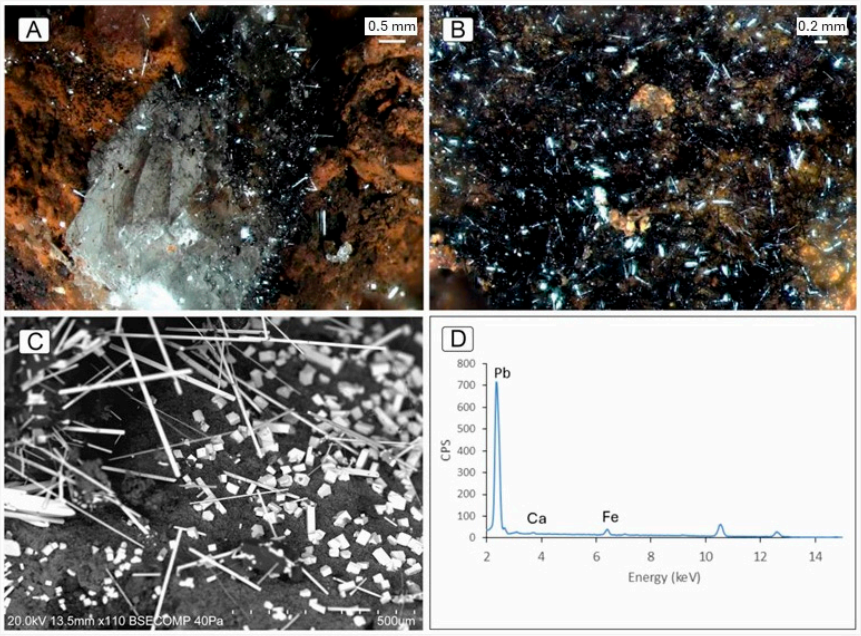


**Figure 6.** Stereomicroscope images of (**A**) black acicular crystals of plattnerite over calcite (sample PR27). (**B**) Detail of plattnerite crystals (PR33). BSE image of plattnerite (**C**). EDS spectra collected in acicular crystals or in parallelepipedal forms are similar (**D**).

### 3.1.2. Goethite, Hematite and Magnetite

Among the Fe-oxy-hydroxides, goethite [$\alpha$-$Fe^{3+}O(OH)$] was the most common mineral found (Table 2), followed by hematite ($Fe_2O_3$). Black magnetite ($Fe^{2+}Fe^{3+}{}_2O_4$) crystals were only observed sporadically (Figure 7A).

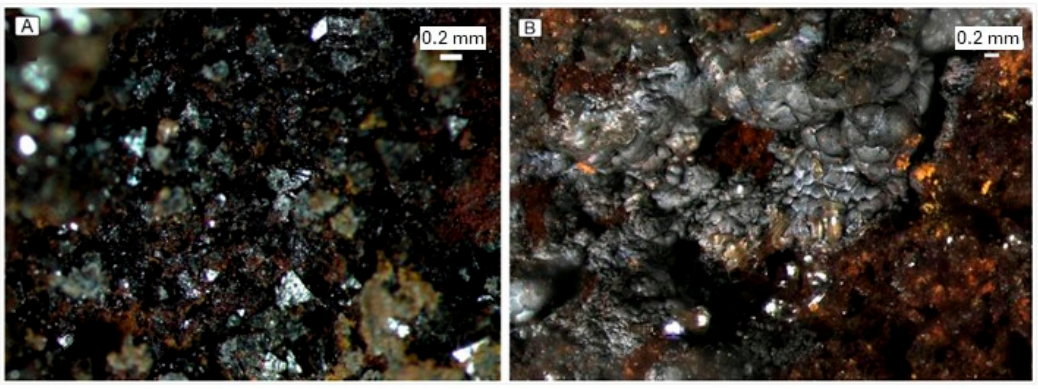


**Figure 7.** Stereomicroscope images of (**A**) magnetite crystals (PR66); (**B**) coronadite (PR70).

3.1.3. Coronadite

Botryoidal aggregates of dark grey coronadite [$Pb(Mn^{4+}{}_6Mn^{3+}{}_2)O_{16}$], the unique manganese mineral observed and already described in the Preguiça mine [25,26], was only detected on the first level (Figure 7B).

3.1.4. Calcite, Smithsonite and Siderite

These carbonate minerals belong to the calcite group, being characterised by their rhombic, prismatic or scalenohedral crystalline structure. Calcite ($CaCO_3$) is very common in the mine and in the mine wastes, presenting variable forms and colours. Some examples can be seen in Figure 8A–D. Although the orange/salmon colour of calcite is usually attributed to the presence of Fe, its content is not very high (about 1%). Pearl-coloured smithsonite ($ZnCO_3$) botryoidal crystals are much less frequent (Figure 8E,F), and the occurrence of $Fe^{2+}$ carbonate siderite ($FeCO_3$) on the analysed fragments is rare.

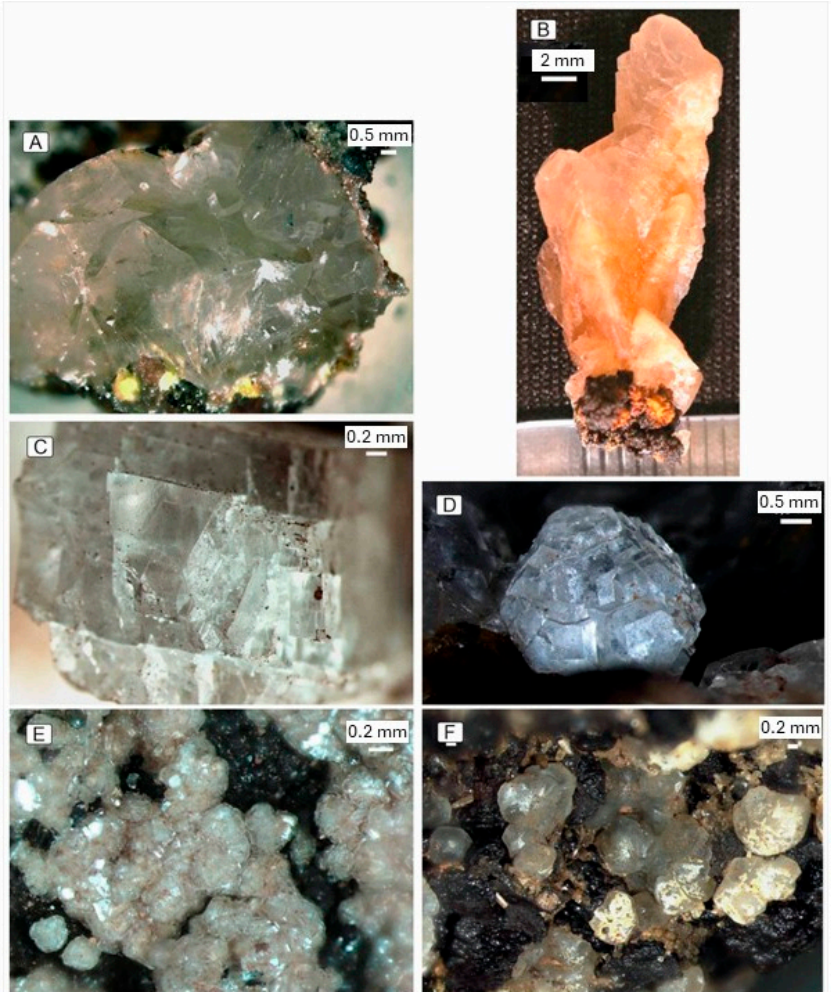


**Figure 8.** Stereomicroscope images and photo of calcite (**A**) from first level (sample PR70); (**B**) orange crystal from third level (PR19); (**C**) third level (PR42); (**D**) fourth level (P4–4); and smithsonite (**E**) from fourth level (P4–1); (**F**) mine waste open pit (PR66).

Hydrozincite, another zinc carbonate [$Zn_5(CO_3)_2(OH)_6$] whose presence was previously described in the Preguiça mine, e.g., [25], was not found.

### 3.1.5. Aragonite and Cerussite

Aragonite ($CaCO_3$), a calcite polymorph (Figure 9A,B), and cerussite ($PbCO_3$) both belong to the aragonite group. The presence of tabular cerussite (Figures 5B and 9C,D) was more frequent than aragonite, particularly in the mine waste open pit.

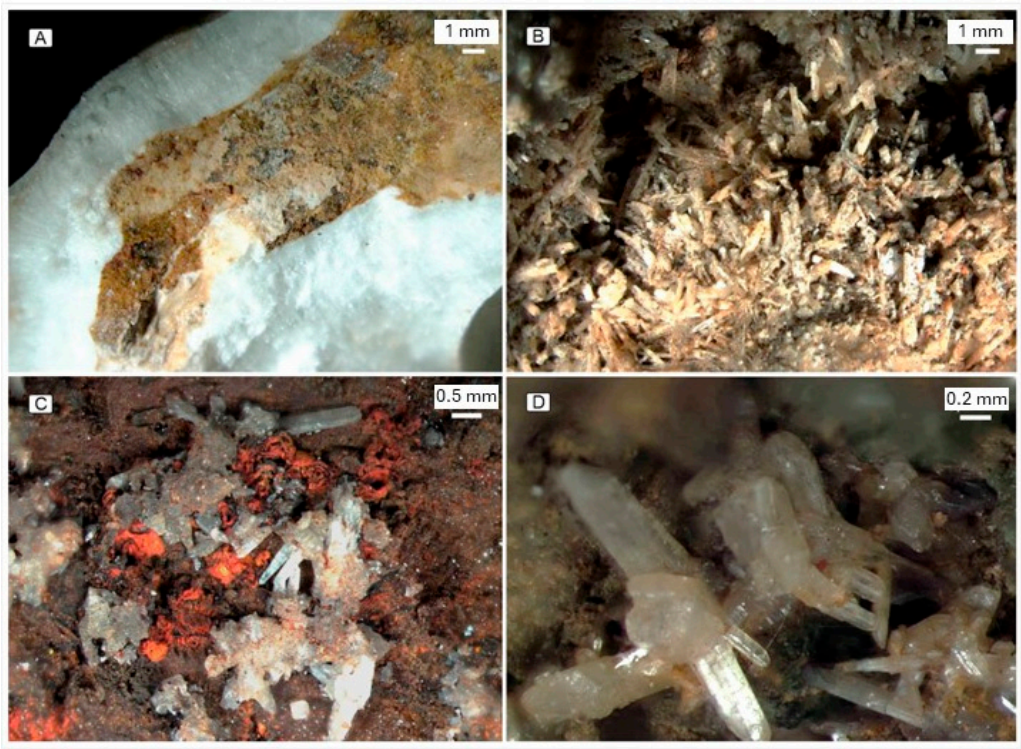


**Figure 9.** Stereomicroscope images of aragonite (**A**) from third level (sample PR53); (**B**) mine waste open pit (PR66–fragment 12); and cerussite from mine waste open pit: (**C**) sample PR66–fragment 3; (**D**) detail of sample PR66–fragment 6.

### 3.1.6. Dolomite, Ankerite and Minrecordite

The minerals dolomite [$CaMg(CO_3)_2$], ankerite [$Ca(Fe^{2+},Mg)(CO_3)_2$] and minrecordite [$CaZn(CO_3)_2$] belong to the dolomite group, being difficult to distinguish by XRD. Therefore, the zinc content obtained through pXRF gives a clue for their identification. Figure 10A shows an example of a dolomite sample with a high zinc content (20%), being probably minrecordite, while Figure 10B shows a brownish sample of calcite plus possibly ankerite.

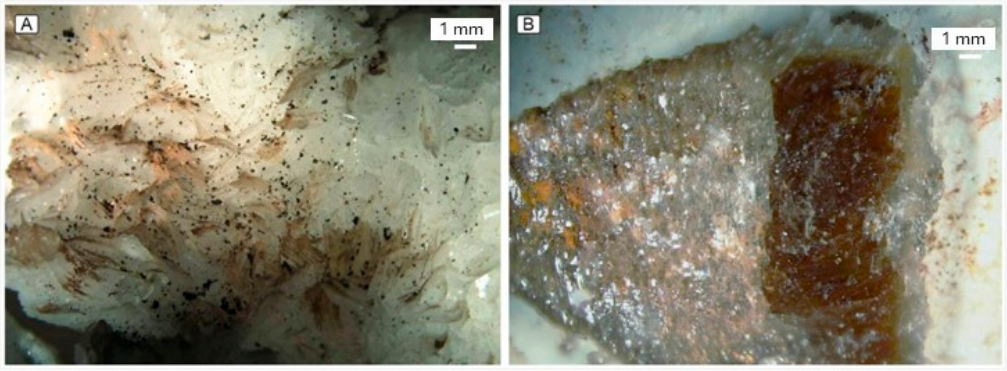


**Figure 10.** Stereomicroscope images of: (**A**) dolomite+minrecordite from third level (sample PR9); (**B**) calcite+ankerite (PR27).

3.1.7. Descloizite, Mottramite and Arsendescloizite

Descloizite, $PbZn(VO_4)(OH)$, mottramite, $PbCu(VO_4)(OH)$, and arsendescloizite, $PbZn(AsO_4)(OH)$, are part of the adelite–descloizite group. The general formula of these orthorhombic minerals is $M1^{1+,2+}M2^{2+,3+}[X^{4+,5+,6+}(O_4,O_3OH)](OH,O)$ where $M1$ = $Na^+$, $Ca^{2+}$, $Cd^{2+}$, $Hg^{2+}$, $Pb^{2+}$; $M2$ = $Mg^{2+}$, $Al^{3+}$, $Mn^{2+,3+}$, $Fe^{2+}$, $Co^{2+}$, $Ni^{2+}$, $Cu^{2+}$, $Zn^{2+}$; $X$ = $Si^{4+}$, $P^{5+}$, $V^{5+}$, $As^{5+}$, $Mo^{6+}$ and solid solutions are very common [35]. Descloizite (zinc–rich) is an end member of a series composed of the mineral mottramite (copper–rich) [36]. Both minerals usually contain significant percentages of both elements: $Pb(Zn, Cu)(VO_4)(OH)$; the ZnO content establishes the classification of the mineral: descloizite (if ZnO > 18%), cuprian descloizite (18% > ZnO > 10%), zincian mottramite (10% > ZnO > 2%) and mottramite (ZnO < 2%). The replacement of V by As is possible, with arsendescloizite being the arsenate analogue of descloizite; Ga and Ge may also be present through incorporation into the crystal structure [37,38].

The first reference to the presence of descloizite in the Preguiça mine and even in Portugal is due to Bensaúde [39]. In that work, a chemical analysis was also published. Several fragments (grey/black, greenish) were identified on the third level (Figure 11A–D); although the XRD spectra usually showed a mixture of minerals, the chemical analysis allowed for a rough estimation of the descloizite composition (disregarding the iron or silica content) in selected fragments. Our results are in accordance with what was published by other authors [38–42] and point out that the majority could be considered descloizite and occasionally cuprian descloizite. Arsendescloizite is also a possibility, as $As_2O_5$ content obtained with pXRF is higher than $V_2O_5$ in some fragments. BSE images of descloizite can be seen in Figure 11E–G, alongside an example of the EDS spectrum collected at various points of the descloizite crystals (Figure 11H).

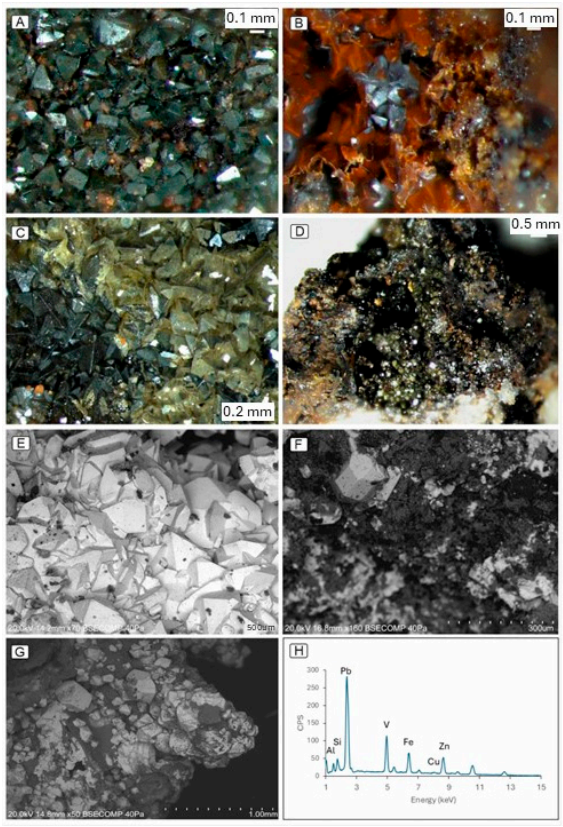


**Figure 11.** Stereomicroscope images of descloizite: (**A**) sample PR38–fragment 12; (**B**) PR59–fragment 2; (**C**) PR47–fragment 4; (**D**) PR46–fragment 3; BSE images of descloizite (**E**–**G**); example of EDS spectrum collected at various points of the descloizite crystals (**H**).

### 3.1.8. Vanadinite and Mimetite

Orange/red vanadinite [$Pb_5(VO_4)_3Cl$], is another vanadium mineral found in the Preguiça mine (Figure 5C), although sporadically. It is a member of the apatite group (apatite supergroup) and forms a solid solution with mimetite [$Pb_5(AsO_4)_3Cl$] (Figures 5D and 12A–D), a frequent yellow mineral (globular or in branching groups in sub-parallel position, tapering down to a point) on the first and third levels. Indeed, lead apatite has the general formula $Pb_5(BO_4)_3(Cl)$, where B = $P^{5+}$ (pyromorphite), $As^{5+}$ (mimetite) and $V^{5+}$ (vanadinite); these three minerals with hexagonal symmetry are the end members of a ternary system and although observed in nature, substitutions of P–As–V are frequent [43–45]. The EDS spectra of the crystals showed the presence of both P and As, but also Ca (Figure 12E,F), leaving the doubt about the presence of mimetite/pyromorphite crystals, phosphohedyphane, or a member of the solid solution.

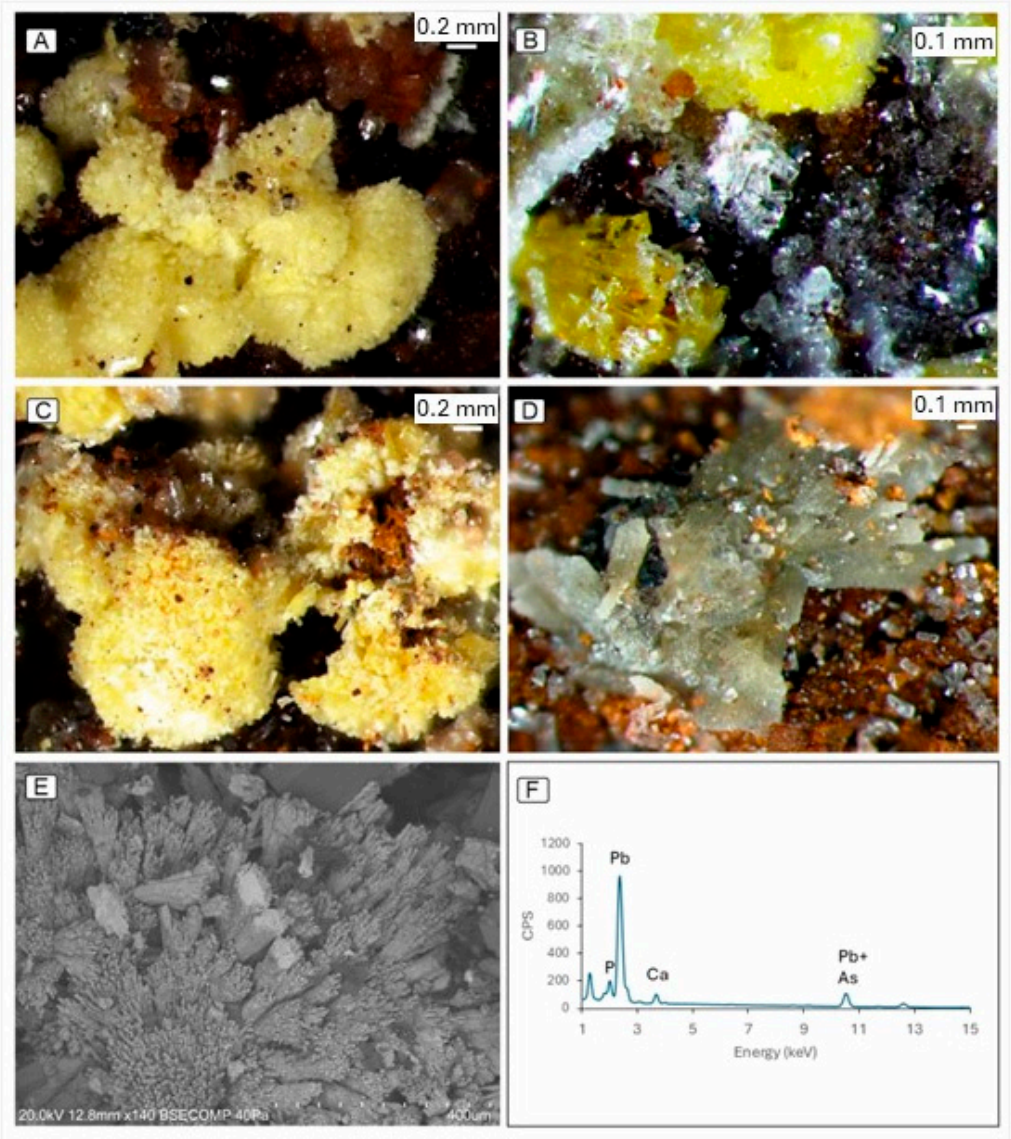


**Figure 12.** Stereomicroscope images of (**A**) yellow mimetite+orange vanadinite+ hyaline willemite (PR70–fragment 3); (**B**) mimetite+willemite (PR68–fragment 1); (**C**) globules of mimetite (PR68–fragment 2); (**D**) greenish crystals of mimetite (PR68–fragment 2); (**E**) BSE image of mimetite; (**F**) example of EDS spectrum collected at various points of the crystals.

3.1.9. Hedyphane and Phosphohedyphane

Hedyphane [$Ca_2Pb_3(AsO_4)_3Cl$] and phosphohedyphane [$Ca_2Pb_3(PO_4)_3Cl$] belong to the hedyphane group (apatite supergroup), with the general formula $Ca_2Pb_3X_3(Cl,OH,F)$, where X is $AsO_4^{3-}$ or $PO_4^{3-}$ [46]. Isomorphic substitution of As for P in the phosphohedyphane structure was noticed [47], and solid solution series among the end members of the apatite and hedyphane groups have already been suggested, e.g., [48,49]: pyromorphite–phosphohedyphane and mimetite–hedyphane. Indeed, the yellow crystals found on the fourth level of the Preguiça mine (Figures 13A and 14) seem to be a mineral from mimetite–hedyphane solid solution, while white crystals (Figure 13B,C) look like hedyphane–phosphohedyphane. SEM images and EDS spectra point to phosphohedyphane crystals [50].

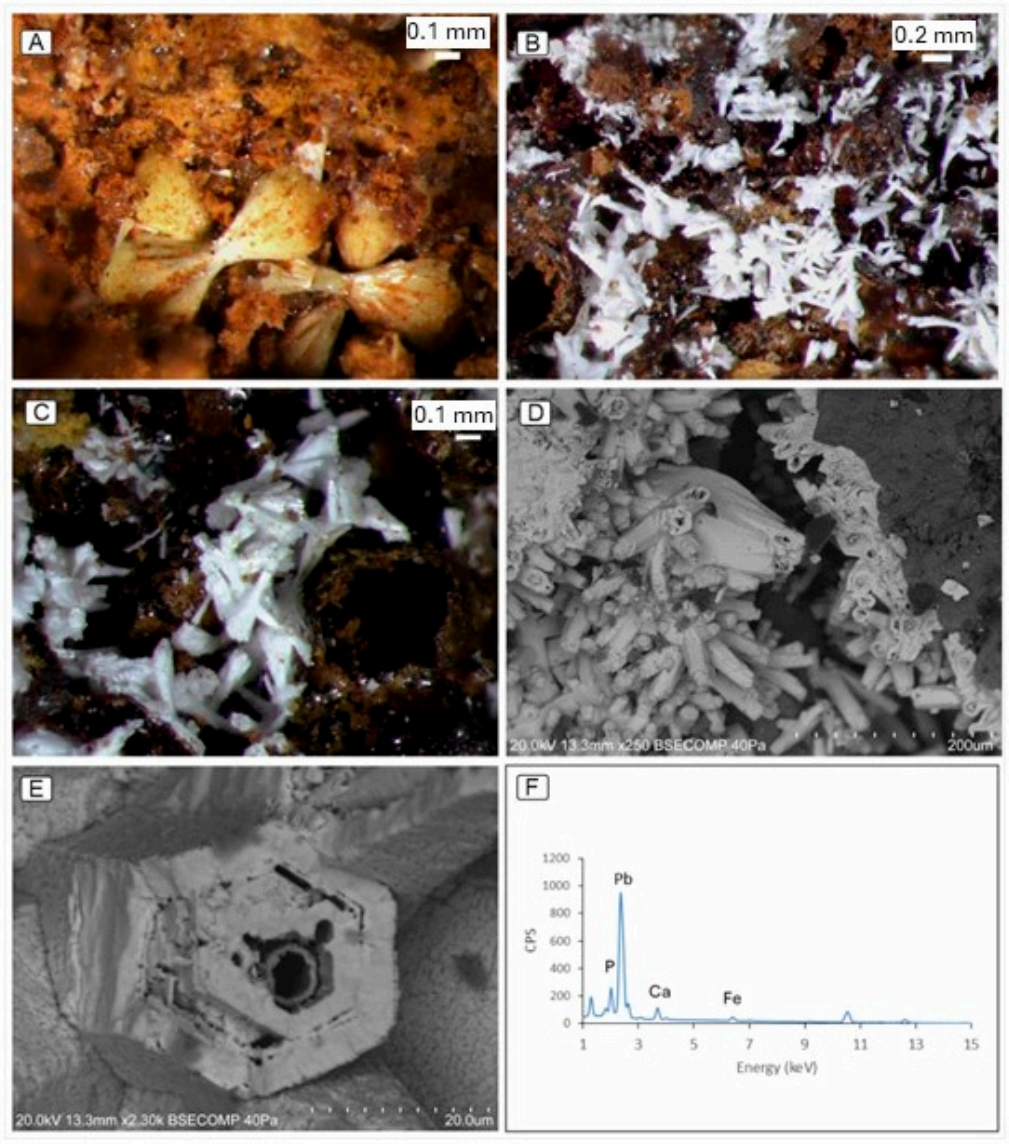


**Figure 13.** Stereomicroscope images of (**A**) branching groups in sub-parallel position of mimetite-hedyphane (P4–10–C); (**B**) phosphohedyphane from the fourth level (P4–10–A); (**C**) detail of the previous image. BSE images of phosphohedyphane (**D**,**E**); (**F**) example of EDS spectrum collected at various points of the crystals.

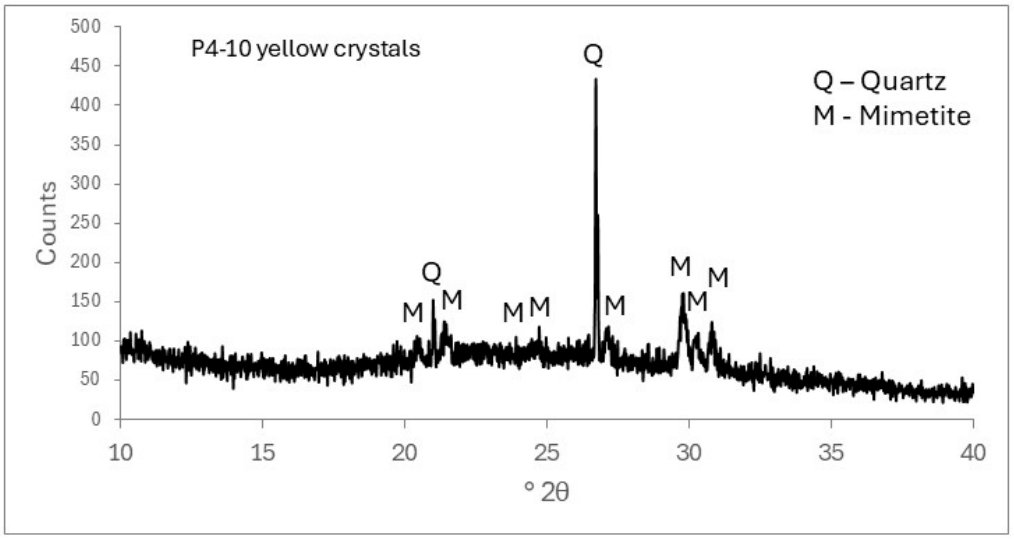


**Figure 14.** XRD spectrum of sample P4–10 with yellow crystals of mimetite-hedyphane. The mineral phases are simplified using the first letter of their name. COD card numbers: Q—1011172; M—1010997.

### 3.1.10. Beudantite

Beudantite ($PbFe_3(AsO_4)(SO_4)(OH)_6$) group belongs to the alunite supergroup. The small brownish masses (Figure 15) were only observed on the fourth mine level. This mineral has been considered a stable host for As and Pb in the environment, e.g., [51].

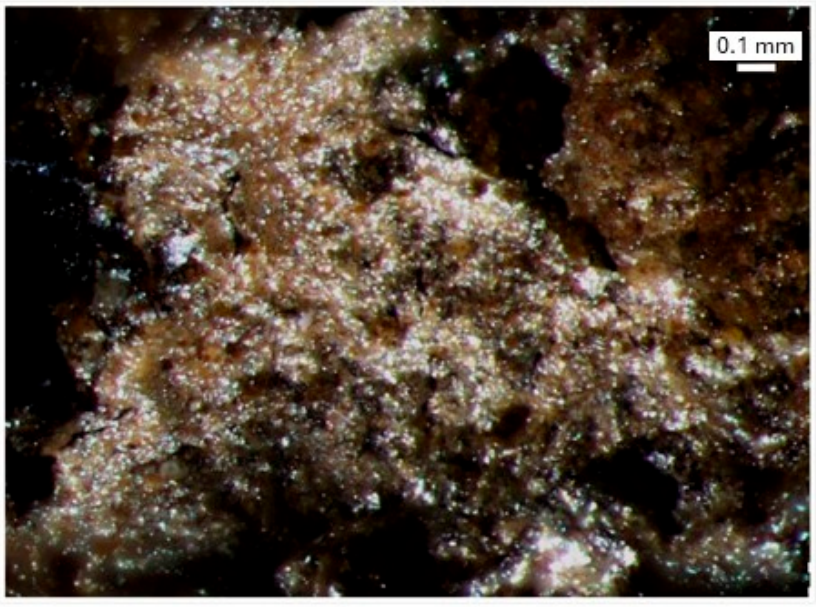


**Figure 15.** Stereomicroscope image of beudantite from fourth level (sample P4–5).

### 3.1.11. Willemite

Willemite ($Zn_2SiO_4$) belongs to the phenakite group and is the most frequent mineral observed on the first level of the mine, also appearing on the third level and in the mine waste open pit, mainly as hyaline, elongated, prismatic crystals (Figure 16A–F). A BSE image of prismatic crystals and the corresponding EDS spectrum are shown in Figure 16G,H. Willemite is a member of the $ZnO–SiO_2–H_2O$ system along with hemimorphite [$Zn_4Si_2O_7(OH)_2 \cdot H_2O$] and sauconite [$Na_{0.3}Zn_3((Si,Al)_4O_{10})(OH)_2 \cdot 4H_2O$] [52]; although hemimorphite has already been described in the Preguiça mine, e.g., [25,29], its presence was not noticed in the present work.

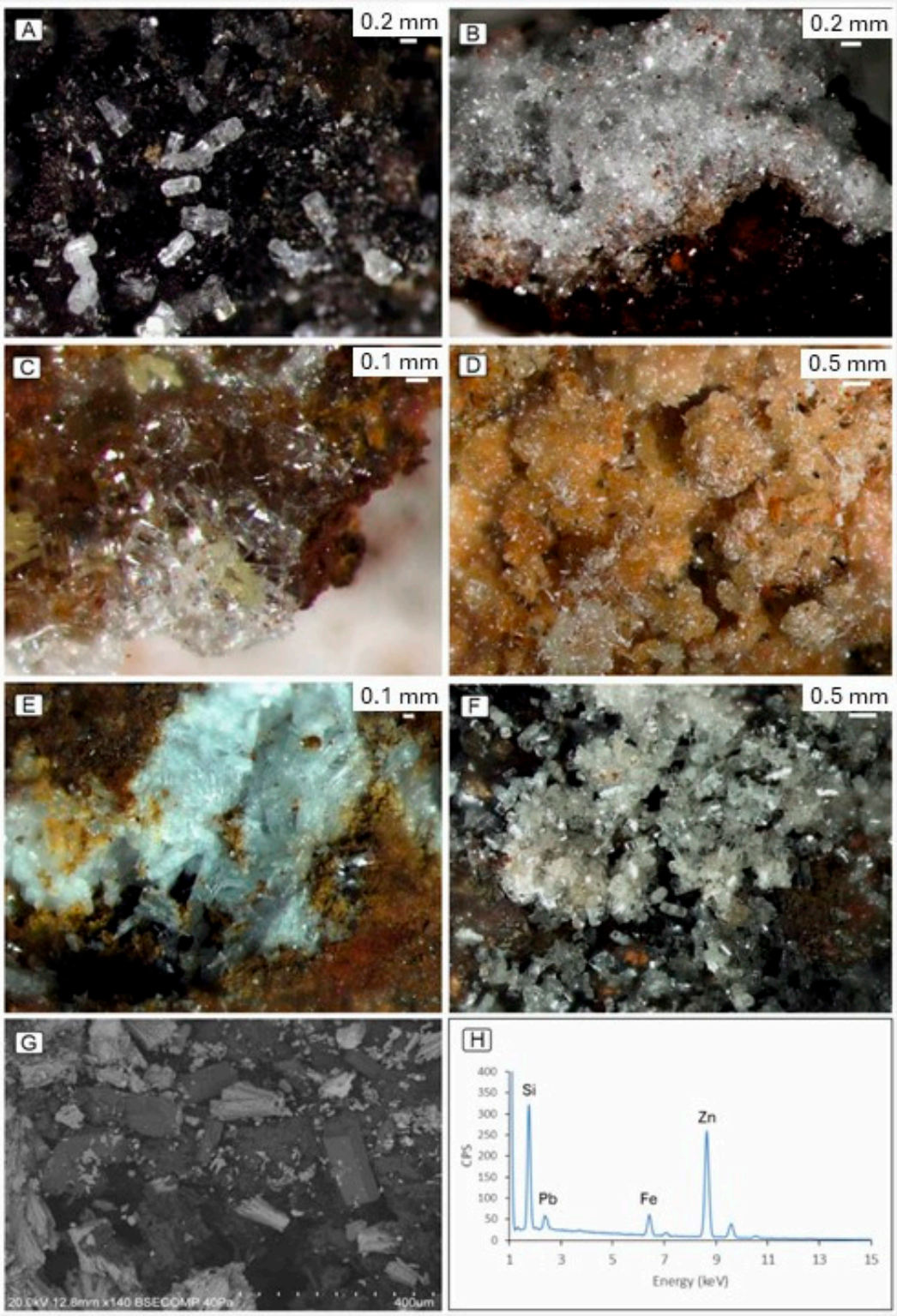


**Figure 16.** Stereomicroscope images of willemite from first level: (**A**) PR69–B; (**B**) PR70–fragment 6G; (**C**) PR70–fragment 6H; (**D**) PR69–A. (**E**) Willemite from third level (PR43–fragment 3A); (**F**) willemite from mine waste open pit (PR66–fragment 3B). BSE image of prismatic crystals of willemite (**G**); example of EDS spectrum (**H**).

### 3.1.12. Fraipontite

Fraipontite [$(Zn,Al)_3((Si,Al)_2O_5)(OH)_4$], a zinc berthierine [$(Fe^{2+},Fe^{3+},Al)_3(Si,Al)_2O_5(OH)_4$], is a rare mineral [53], belonging to the kaolinite–serpentine group (serpentine subgroup). Fe, Cu, Mg, Ca and K may be present in traces. Massive silky whitish and greenish fraipontite

was identified (Figures 17 and 18) on the third level of the Preguiça mine. The approximate chemical compositions of the two samples, in which only fraipontite was identified by XRD, are presented in Table 3. The greenish colour observed could be due to a copper-bearing variety of fraipontite [54]. SEM data (Figure 17E–H) confirm this idea, as the spectrum of the greenish sample, in comparison with the whitish one, displays Cu and Fe peaks. It is also noteworthy that Zn level is higher in the greenish sample and Al is lower. The presence of vestigial Ca is noticed in both samples. These results are in accordance with data from other authors, e.g., [53,54]. Indeed, the presence of fraipontite/sauconite in the Preguiça mine has already been mentioned as a new interstratified clay mineral with fraipontite contents of about 70 to 90% [55].

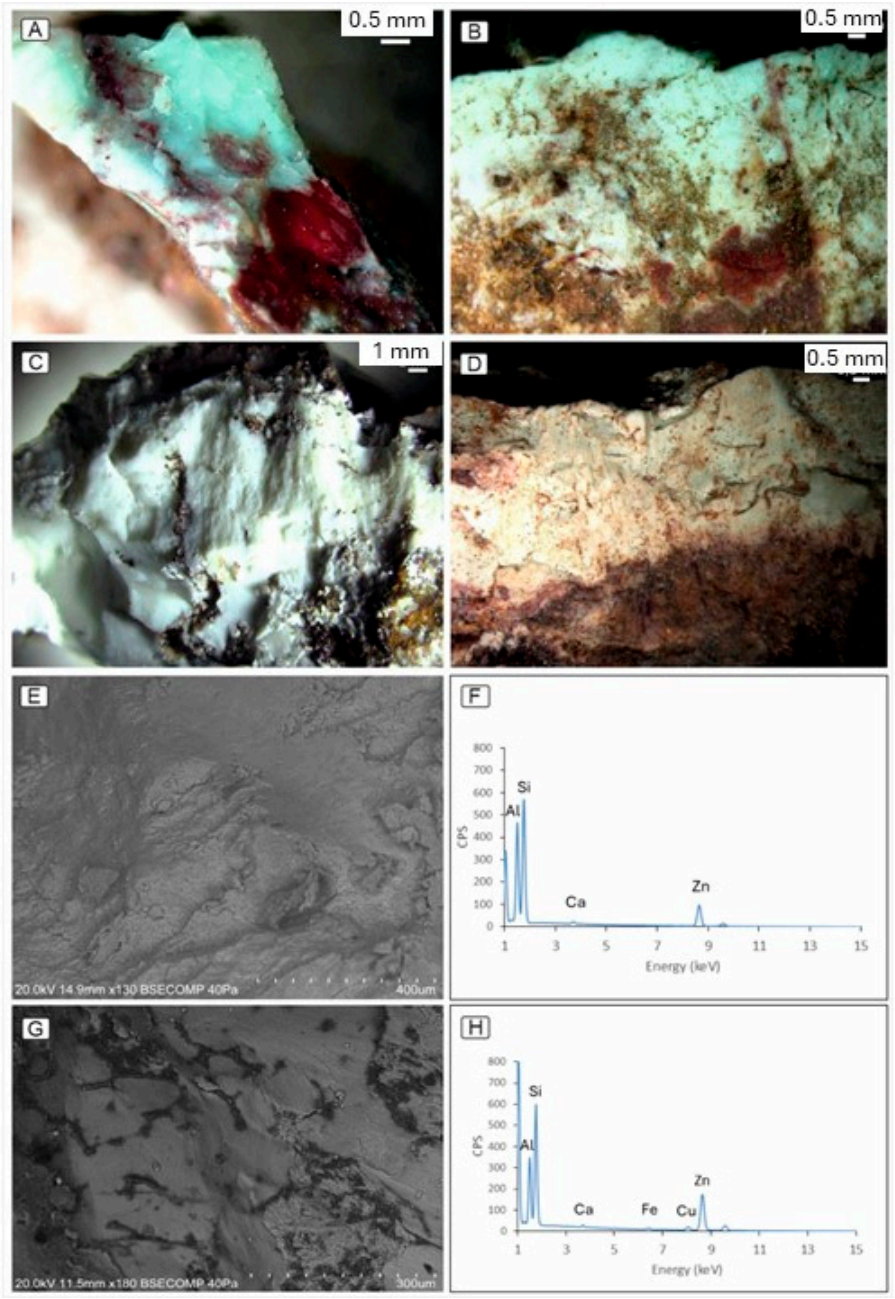


**Figure 17.** Stereomicroscope images of fraipontite from third level: (**A**) sample PR24A; (**B**) PR24B; (**C**) PR41A; (**D**) PR24C. BSE image and EDS spectrum of massive fraipontite: whitish (**E**,**F**); greenish (**G**,**H**).

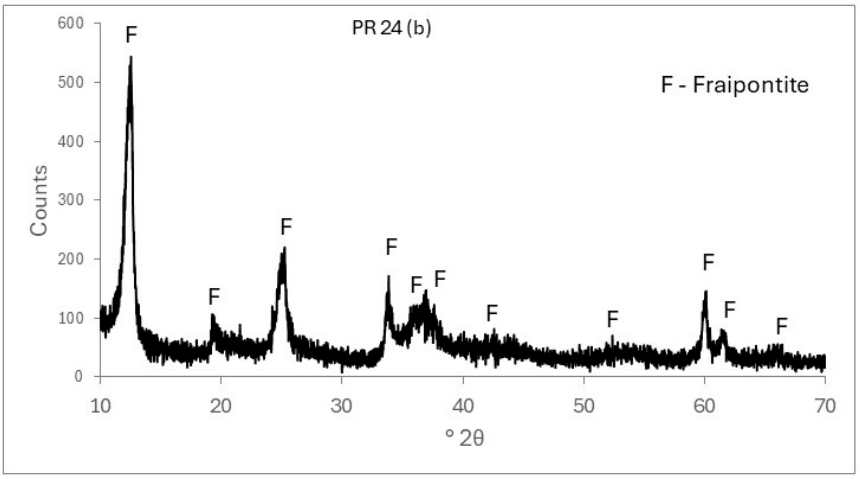


**Figure 18.** XRD spectrum of a greenish massive sample from the third level (PR24B). PDF card number: 00-034-0782.

**Table 3.** Approximate chemical composition (% major elements) obtained by pXRF; - means not detected.

| | $SiO_2$ | $Al_2O_3$ | $Fe_2O_3$ | ZnO | CuO | Total |
|---|---|---|---|---|---|---|
| PR24B (greenish) | 15 | 4 | 6 | 62 | 4 | 91 |
| PR41A (whitish) | 26 | 11 | 3 | 51 | - | 91 |

### 3.1.13. Gypsum

Gypsum crystals ($CaSO_4 \cdot 2H_2O$), one of the most common sulphate minerals, were observed on the third and fourth levels (Figure 19), associated with calcite, smithsonite, jarosite or epsomite.

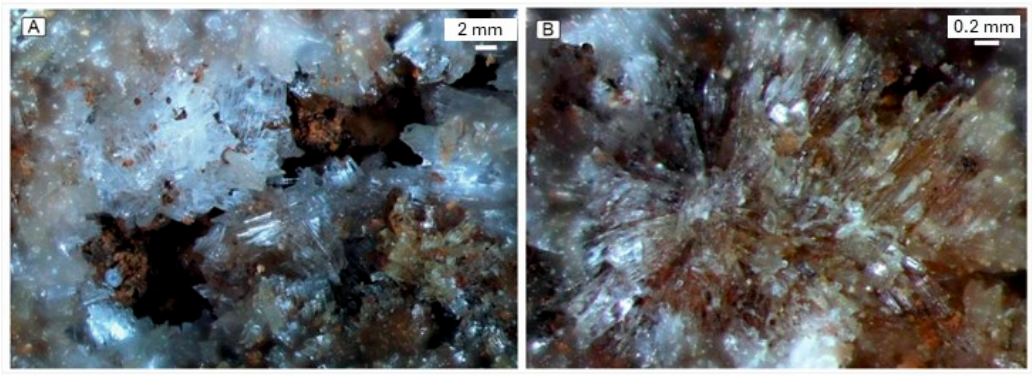


**Figure 19.** Stereomicroscope images of gypsum from fourth level: (**A**) sample P4–16A; (**B**) P4–16C.

## *3.2. Geochemical Characterisation*

Chemical analyses were performed on the bulk samples as collected (see Supplementary Materials S1), allowing us to determine the major elemental concentrations and relate them to the observed mineralogy. Indeed, pXRF equipment is a useful tool for a quick and inexpensive overview of a wide range of elements, but a previous check of the precision and accuracy of the equipment must be done. The comparison between concentrations obtained using pXRF for various international reference standards and their published chemical contents allow us to evaluate analytical accuracy. Details of the applied methodology are presented in [56,57]. Additionally, the XRF spectra of some samples were visualised to really verify the presence of elements in minor or vestigial contents (examples in S1).

Considering that the obtained concentrations are only approximate, the major values obtained in decreasing order are Fe (63%), Ca (61%), Zn (59%), Pb (41%), Si (41%), S (36%),

Mg (16%), Cu (15%), Al (12%), V (8%), Mn (3%), As (3%), Sb (2%), K (1%), P (1%), Cr (0.9%), Cd (0.3%), Ba (0.3%), Ti (0.2%), Co (0.1%), Ta (0.1%), Sr (0.07%), Rb (0.06%), Zr (0.06%), W (0.06%), Ag (0.05%), Hg (0.05%), Bi (0.04%), Sn (0.03%), Ga (0.03%) and Au (0.03%). The very low values of Tl, Ni, Mo, Y, Nb, Se, Th, U and REE were not considered. From previous studies [56], some contents are obtained by excess, namely, Ca, Zn, Pb, S, Cu, Mn, As, Sb, K, Sr, Rb, W, Ni, Mo and Se, and others, namely, Fe, Mg, Al, Ba and Ga, by default; the Si and Ti values are real. The lowest reliability measurements will be for V, P, Cr, Cd, Co, Ta, Zr, Ag, Hg, Bi, Sn, Au, Tl, U and REE.

These results are, in general, in accordance with the mineral phases identified. The main Zn- and Pb-bearing mineral phases present in the samples included smithsonite ($ZnCO_3$), willemite ($Zn_2SiO_4$), fraipontite [$(Zn,Al)_3((Si,Al)_2O_5)(OH)_4$], minrecordite [$CaZn(CO_3)_2$], descloizite [$PbZn(VO_4)(OH)$], plattnerite ($PbO_2$), cerussite ($PbCO_3$), mimetite [$Pb_5(AsO_4)_3Cl$] and hedyphane [$Ca_2Pb_3(AsO_4)_3Cl$], with the presence of descloizite, willemite and mimetite being more frequent among these supergene minerals [29]. The highest content obtained for Zn and Pb in the studied samples is related with the presence of smithsonite and descloizite respectively.

In the lead vanadate minerals, descloizite [$PbZn(VO_4)(OH)$], mottramite [$PbCu(VO_4)(OH)$] and vanadinite [$Pb_5(VO_4)_3Cl$], V is in the oxidation state +5, forming ($VO_4$) tetrahedra [43,58,59], and according to the last authors, V may be critical for the transition to electric cars, as a component within Li-ion batteries [$Li_3V_2(PO_4)_3$]. These minerals have a high density, they are non-conductors and non-magnetic, and they have weak to negative magnetic susceptibility [60]. As reported, the Preguiça mine vanadate minerals precipitate from V-bearing solutions, e.g., [25], with their presence also assigned in southern Africa (Namibia, Zambia and Angola), associated with low-temperature, non-sulphide mineralisation [61]. Vanadium (V) is included in the most recent list of critical and strategic raw materials (CRM and SRM) [2]. Given the growing demand for these materials due to their wide range of industrial applications, the concentrations obtained for the Preguiça mine samples (S1), which have to be confirmed by other analytical methods, highlight the potential value of a more detailed future investigation. Vanadium (classified as a CRM) is used primarily in high-strength alloys for applications in aeronautics, space technology, and nuclear reactors, and it also serves as an important chemical catalyst. Fe-oxy-hydroxides (e.g., goethite or hematite) have the capability to host a wide range of elements, depending on the chemistry of the primary deposit and on the properties of the fluids [[62] and references herein]; these authors report that FeO/OH associated with supergene non-sulphide mineralisation is commonly enriched in Zn and Pb with traces of As, Cd, Co, Cu, Ga, Ge, Hg, In, Mo, Ni, Sb, Sc and V. Antimony, for example, is recognised as a valuable indicator in geochemical prospecting surveys [63,64]. It occurs in different oxidation states in nature (−3, 0, +3 and +5) and can substitute for Bi, Pb, As, Cu, Ag and S in various minerals [65]. Sb is considered a CRM and is commonly used as flame retardant, in defence applications, and in lead–acid batteries [2].

Mimetite, [$Pb_5(AsO_4)_3Cl$], according to the results obtained in this work, is the main source for As, a CRM with applications in semiconductors and alloys. On the other hand, Sr seems to be more related with aragonite then calcite in substitution of Ca. However, dolomite is the main source of Mg, an SRM used, for example, in lightweight alloys for automotive, electronics, packaging or in construction and as a desulphurization agent in steelmaking.

## 4. Conclusions

This study provides new insights into the mineralogical and geochemical characterisation of samples from the old Preguiça mine (Beja, Portugal), highlighting the phase distribution associated with the historical Fe–Zn–Pb deposit. The various mineral phases identified on the different four mine levels and in waste materials demonstrate the miner-

alogical diversity generated by supergene alteration processes acting on primary sulphide mineralisation hosted in dolomitic limestones.

Although remnants of primary sulphides (i.e., pyrite, marcasite, chalcopyrite, sphalerite and galena) are scarce, the mine is dominated by a wide range of secondary oxides (Si, Mn, Fe and Pb), carbonates (Mg, Ca, Fe, Zn and Pb), arsenates (Ca, Fe, Zn, and Pb), vanadates (Cu, Zn, and Pb), silicates (Na, Mg, Al, K, Ca, Fe, and Zn), phosphates (Ca and Pb) and sulphates or hydroxysulphates (Mg, K, Ca, Fe, Zn and Pb). The following mineral phases can be emphasised: goethite, hematite, calcite, dolomite, descloizite (vanadate of lead and zinc), willemite (zinc silicate), mimetite (lead arsenate), cerussite (lead carbonate) and smithsonite (zinc carbonate); these denote the complexity of the processes involved in their formation and the capacity to carrier/concentrate possibly valuable elements. Two less commonly reported minerals, fraipontite (a Zn-rich clay mineral) and massicot (PbO), whose presence has not previously been described at the Preguiça mine, were also identified, contributing to a more comprehensive understanding of the mine's mineralogical diversity.

It is also worth noting that pXRF proved to be a reliable, cost-effective tool for a rapid evaluation of many elements of interest. Bulk geochemical analyses generally reflect the observed mineralogy, with high concentrations of Fe, Ca, Zn, and Pb corresponding to the presence of iron oxides (hematite and goethite), carbonates (calcite and dolomite), and Zn- and Pb-bearing supergene minerals, mainly descloizite, willemite, and mimetite.

The results also highlight the presence of several critical and strategic raw materials, particularly V and As, which are associated with vanadate and arsenate minerals such as descloizite and mimetite. The occurrence of Sb, Sr, and other potentially valuable elements within secondary minerals suggests that the supergene alteration zone of the Preguiça deposit may represent a promising target for further detailed geochemical and mineralogical investigations. The sustainable recovery of such elements also contributes to the mitigation of environmental risks associated with the presence and mobility of Pb-, Zn-, and As-bearing secondary minerals, highlighting the importance of future research to better understand contaminant dispersion and geochemical stability, particularly in the case of the waste pile. Indeed, this Preguiça mine study demonstrates the relevance of revisiting other abandoned mining areas within a sustainable and strategic raw material framework.

**Supplementary Materials:** The following supporting information can be downloaded at: https://www.mdpi.com/article/10.3390/min16040348/s1, S1: Chemical analysis and pXRF spectra.

**Author Contributions:** Conceptualization, T.P.S., I.M., and S.S.; methodology, T.P.S., I.M., S.S., I.R., and J.M.; validation, T.P.S., I.M., S.S., D.P.S.d.O., I.R., and J.M.; formal analysis, T.P.S., I.M., and D.P.S.d.O.; investigation, T.P.S., I.M., and S.S.; writing—original draft preparation, T.P.S., I.M., and S.S.; writing—review and editing, T.P.S., I.M., S.S., D.P.S.d.O., I.R., and J.M.; project administration, D.P.S.d.O.; funding acquisition, D.P.S.d.O. All authors have read and agreed to the published version of the manuscript.

**Funding:** This research was partly funded by the Geological Service for Europe project (GSEU), Grant Agreement number 101075609—GSEU—HORIZON-CL5-2021-D3-02.

**Data Availability Statement:** The original contributions presented in this study are included in the article/Supplementary Materials. Further inquiries can be directed to the corresponding author.

**Acknowledgments:** The authors would like to thank Ricardo Pimentel for providing an article of his authorship related to the Preguiça mine.

**Conflicts of Interest:** Author Ivo Rodrigues was employed by the EDIA. The remaining authors declare that the research was conducted in the absence of any commercial or financial relationships that could be construed as a potential conflict of interest.

## References


1. Conceição, F.T.; Vasconcelos, P.M.; Godoy, L.H.; Navarro, G.R.B.; Montibeller, C.C.; Sardinha, D.S. Water/rock interactions, chemical weathering and erosion, and supergene enrichment in the Tapira and Catalão I alkaline-carbonatite complexes. *Braz. J. Geochem. Explor.* **2022**, *237*, 106999. [CrossRef]
2. Grohol, M.; Veeh, C.; European Commission. *Study on the Critical Raw Materials for the EU 2023: Final Report*; Publications Office of the European Union: Luxembourg, 2023. Available online: https://data.europa.eu/doi/10.2873/725585 (accessed on 29 August 2025).
3. Blengini, G.A.; Nuss, P.; Dewulf, J.; Nita, V.; Peirò, L.T.; Vidal-Legaz, B.; Latunussa, C.; Mancini, L.; Blagoeva, D.; Pennington, D.; et al. EU methodology for critical raw materials assessment: Policy needs and proposed solutions for incremental improvements. *Resour. Policy* **2017**, *53*, 12–19. [CrossRef]
4. Mateus, A.; Noronha, F. Mineral deposits of Portugal. In *Geology of Portugal, Volume II: Historical Evolution*; Noronha, F., Mateus, A., Eds.; Escolar Editora: Lisbon, Portugal, 2010.
5. Nordstrom, D.K. Mine waters: Acidic to circumneutral. *Elements* **2011**, *7*, 393–398. [CrossRef]
6. Oliveira, J.T.; Oliveira, V.; Piçarra, J.M. Traços gerais da evolução tectono-estratigráfica da Zona de Ossa Morena, em Portugal. *Cuad. Lab. Xeolóxico Laxe* **1991**, *16*, 221–250.
7. Oliveira, J.T.; Quesada, C.; Pereira, Z.; Matos, J.X.; Solá, A.R.; Rosa, D.; Albardeiro, L.; Díez-Montes, A.; Morais, I.; Inverno, C.; et al. South Portuguese Terrane: A Continental Affinity Exotic Unit. In *The Geology of Iberia: A Geodynamic Approach. Regional Geology Reviews*; Quesada, C., Oliveira, J., Eds.; Springer: Cham, Switzerland, 2019; pp. 173–206. [CrossRef]
8. Mateus, A.; Figueiras, J.; Oliveira, V.; Matos, J.X. Recrystallised (Fe-) Zn- Pb ores of the Portel-Ficalho region (Ossa Morena Zone, Portugal). *Ciências Terra UNL Lisb.* **2003**, *V*, F86–F89.
9. Piçarra, J.; Oliveira, V.; Silveira, A.; Barbosa, B. *Notícia Explicativa da Carta Geológica da Folha 44-A, Amareleja. Escala 1/50 000*; Instituto Nacional de Engenharia, Tecnologia e Inovação: Lisboa, Portugal, 2007; 47p. Available online: https://geoportal.lneg.pt/pt/dados_abertos/cartografia_geologica/cgp50k/44-A (accessed on 25 February 2026).
10. Goinhas, J.A.C. Estudo geológico-económico preliminar dos jazigos de Zn/Pb da região de Portel (Alentejo). In *I Congresso Hispano-Luso-Americano de Geologia Económica, Madrid, Spain, 19–23 September 1971, Lisboa, Portugal, 24–25 September 1971*; Imprenta Ibérica: Barcelona, Spain, 1971; Volume 4, pp. 621–642.
11. Oliveira, V.; Piçarra, J.M. Litoestratigrafia do Anticlinório de Moura-Ficalho (Zona Ossa Morena). *Maleo Bol. Inf. Soc. Geol. Port.* **1986**, *2*, 33. Available online: https://eu-central-1.linodeobjects.com/socgeol-files/production/documents/214/original.pdf?1651938579 (accessed on 25 February 2026).
12. Matos, J.; Rosa, C. *Diagnóstico Preliminar de Minas Abandonadas—Área Sul*; Relatório interno IGM: Lisboa, Portugal, 2001; 276p.
13. Carvalhosa, A. *Carta Geológica à Escala 1/5 000. Notícia Explicativa da Folha 40-D*; Serviços Geológicos de Portugal: Lisboa, Portugal, 1967. Available online: https://geoportal.lneg.pt/pt/dados_abertos/cartografia_geologica/cgp50k/40-D (accessed on 25 February 2026).
14. Gonçalves, P.; Matos, J.X.; Quental, L.; Batista, M.J.; Marques, F.; Sousa, P.; Morais, I.; Albardeiro, L. Remote sensing and thematic mapping applied to mineral exploration in the Moura-Ficalho base metals mining region, Ossa-Morena Zone, Portugal. *Geophys. Res. Abstr.* **2019**, *21*, EGU2019-9428.
15. Patinha, C.A.F. Impacto de Elementos Vestigiais na Envolvente de Antigas Explorações Mineiras Utilizando Meios Amostrais Diferenciados. Contribuição Para o Conhecimento Dos Mecanismos de Dispersão e Fixação dos Elementos Cu, Pb, Zn e As em Meio Superficial. Ph.D. Thesis, Universidade de Aveiro, Aveiro, Portugal, 2002.
16. Faria, F. *Área de Prospecção de Moura-Ficalho*; Rel. Téc. Arquivo INETI: Lisboa, Portugal, 2001.
17. Gomes, A.A.R.; Barros, J.J.O.; Araújo, C. Formações zincíferas da Serra da Preguiça. *Est. Not. Trab. S.F.M.* **1958–1959**, *XIII*, 47–64.
18. Tornos, F.; Inverno, C.M.; Casquet, C.; Mateus, A.; Ortiz, G.; Oliveira, V. The metallogenic evolution of the Ossa-Morena Zone. *J. Iber. Geol.* **2004**, *30*, 143–181.
19. Bottaini, C.E.; Vilaça, R.; Serra, M. A metalurgia Pré e Proto-Histórica do concelho de Moura: Contributo para o seu estudo. *Lacant—Rev. História Arqueol. Património* **2025**, *8*, 5–22. Available online: https://www.cm-moura.pt/lacant/RevistaLacant8.pdf (accessed on 25 February 2026).
20. Silva, J.M.; Araújo, C. Estudo da concessão Umbria da Preguiça e dos campos livres Herdade da Preguiça, sítio do Álamo e Herdade do Álamo. *Est. Not. Trab. S.F.M.* **1948**, *IV*, 197–209.
21. Gomes, A.A.R.; Barros, J.J.O.; Araújo, C. Minas de Ferro da Preguiça N. º 6 e Serra da Abelheira. *Est. Not. Trab. S.F.M.* **1959**, *XIII*, 39–46. Available online: https://docbase.lneg.pt/docs/EstudosNotasTrabalhos/Vol13Fasc1e2_Abelheiro.pdf (accessed on 25 February 2026).
22. Da Silva, A.C.; Triantafyllou, A.; Delmelle, N. Portable x-ray fluorescence calibrations: Workflow and guidelines for optimizing the analysis of geological samples. *Chem. Geol.* **2023**, *623*, 121395. [CrossRef]
23. Johnson, L.R.M.; Ferguson, J.R.; Freund, K.P.; Drake, L.; Duke, D. Evaluating obsidian calibration sets with portable X-Ray fluorescence (ED-XRF) instruments. *J. Archaeol. Sci. Rep.* **2021**, *39*, 103126. [CrossRef]

24. Li, Z.; Wei, N.; Li, M.; Wu, S.; Li, H.; Liu, P. Application of Portable X-Ray Fluorescence Analysis in Mineral Exploration: A Case Study from Cimabanshuo Porphyry Copper Deposit. *Minerals* **2025**, *15*, 1286. [CrossRef]
25. Martins, A.M.I. Mining Field of Preguiça and Herdade de Vila Ruiva. Available online: https://www.mindat.org/article.php/1798/Mining+field+of+Pregui%C3%A7a+and+Herdade+de+Vila+Ruiva (accessed on 15 July 2025).
26. Rosell, J.; Viñals, J.; Clemente, F.; Alcuña, F.J. Mina da Preguiça, Lead and Zinc Supergenic Minerals. Freguesia de Sobral da Adiça, Concelho de Moura, Beja, Alentejo, Portugal. *Rev. Miner.* **2008**, *III*, 6–20. (In Spanish)
27. Quental, L. *Mineralogical Characterization of Ferruginous Concentrations and Soils in the Area of the Vila Ruiva and Preguiça Mines*; IGM (Instituto Geológico e Mineiro): Lisbon, Portugal, 1995.
28. Costa, Ó.; Marinho Reis, P.; Nogueira, P.; Pimenta Simões, P.; Kumoleha, A. Mineralogical and geochemical characterization of surface soils and waste piles collected in the Preguiça-Vila Ruiva mining area. *Comun. Geol.* **2025**, *112*, 345–349. [CrossRef]
29. Pimentel, R.; Nunes, R.; De Ascenção, R. Les minéraux d'altération de plomb (Pb) et zinc (Zn) du massif de Preguiça, Moura, Portugal. *Règne Minér.* **2007**, *75*, 19–26.
30. Goienaga, N.; Arrieta, N.; Carrero, J.A.; Olivares, M.; Sarmiento, A.; Martinez-Arkarazo, I.; Fernández, L.A.; Madariaga, J.M. Micro-Raman spectroscopic identification of natural mineral phases and their weathering products inside an abandoned zinc/lead mine. *Spectrochim. Acta Part A* **2011**, *80*, 66–74. [CrossRef]
31. Iavazzo, P.; Adamo, P.; Boni, M.; Hillier, S.; Zampella, M. Mineralogy and chemical forms of lead and zinc in abandoned mine wastes and soils: An example from Morocco. *J. Geochem. Explor.* **2012**, *113*, 56–67. [CrossRef]
32. Takahashi, T. Supergene alteration of zinc and lead deposits in limestone. *Econ. Geol.* **1960**, *55*, 1083–1115. [CrossRef]
33. Kusha, H. Plattnerite from Kupferschiefer, Poland, and its meaning for mineralizing conditions. *Ann. Soc. Geol. Pol.* **1998**, *68*, 279–285.
34. Heddle, M.F. On Dudgeonite, Hydroplumbite, Plumbonacrite and Plattnerite. *Min. Mag.* **1889**, *8*, 200–203. [CrossRef]
35. Đorđević, T.; Kolitsch, U.; Nasadala, L. A single-crystal X-ray and Raman spectroscopic study of hydrothermally synthesized arsenates and vanadates with the descloizite and adelite structure types. *Am. Mineral.* **2016**, *101*, 1135–1149. [CrossRef]
36. Frost, R.L.; Xi, Y.; López, A.; Corrêa, L.; Scholz, R. The molecular structure of the vanadate mineral mottramite [PbCu($VO_4$)(OH)] from Tsumeb, Namibia—A vibrational spectroscopic study. *Spectrochim. Acta Part A Mol. Biomol. Spectrosc.* **2014**, *122*, 252–256. [CrossRef]
37. Reddya, S.L.; Reddy, B.J.; Frost, R.L. Spectroscopic investigations of descloizite. *Spectrochim. Acta Part A* **2009**, *72*, 194–197. [CrossRef]
38. Millman, A.P. The descloizite-mottramite series of vanadates from Minas do Lueca, Angola. *Am. Mineral.* **1960**, *45*, 763–773.
39. Bensaúde, A. Note sur la descloizite de la mine de Preguiça (Sobral da Adiça). *Bull. Société Port. Des. Sci. Nat.* **1920**, *VIII*, 154–156.
40. Aires-Barros, L. Estudo radiográfico e por espectrografia dos raios infravermelhos, de descloizite, libetenite e atacamite das minas da Preguiça, Vieiros e Bogalho (Alentejo). *Bol. Soc. Geol. Port.* **1969**, *XVII*, 51–64.
41. Von Rahden, H.V.R.; Dicks, L.W.R. Descloizite, mottramite and vanadinite from South West Africa: An infrared and X-ray study. *Am. Mineral.* **1967**, *52*, 1067–1076.
42. Liso, M.J.; Leon, M.; Murciego, A.; Rodriguez, M.A. La descloicita cúprica de Santa Marta, (Badajoz, SW de España); un studio comparative de las técnicas de caracterización en la serie descloicita-motramita. *Comun. Inst. Geol. Min.* **1994**, *80*, 51–56.
43. Laufek, F.; Skála, R.; Haloda, J.; Císařová, I. Crystal structure of vanadinite: Refinement of anisotropic displacement parameters. *J. Czech Geol. Soc.* **2006**, *51*, 271–275. [CrossRef]
44. Antao, S.M.; Dhaliwal, I. Lead apatites: Structural variations among $Pb_5(BO_4)_3Cl$ with *B* = P (pyromorphite), As (mimetite) and V (vanadinite). *J. Synchrotron Rad.* **2018**, *25*, 214–221. [CrossRef]
45. Solecka, U.; Puzio, B.; Kersten, M.; Topolska, J.; Manecki, M.; Bajda, T. Solubility of mimetite $Pb_5(AsO_4)_3Cl$—Vanadinite $Pb_5(VO_4)_3Cl$ solid solution series at 5–65 °C. *Chem. Geol.* **2025**, *675*, 122609. [CrossRef]
46. Pasero, M.; Kampf, A.R.; Ferraris, C.; Pekov, I.V.; Rakovan, J.; White, T.J. Nomenclature of the apatite supergroup minerals. *Eur. J. Mineral.* **2010**, *22*, 163–179. [CrossRef]
47. Frost, R.L.; Scholz, R.; López, A.; Firmino, B.E.; Lana, C.; Xi, Y. A Raman and infrared spectroscopic characterisation of the phosphate mineral phosphohedyphane $Ca_2Pb_3(PO_4)_3Cl$ from the Roote mine, Nevada, USA. *Spectrochim. Acta Part A Mol. Biomol. Spectr.* **2014**, *127*, 237–242. [CrossRef] [PubMed]
48. Rouse, R.C.; Dunn, P.J.; Peacor, D.R. Hedyphane from Franklin, New Jersey and Långban, Sweden: Cation ordering in an arsenate apatite. *Am. Mineral.* **1984**, *69*, 920–927.
49. Markl, G.; Marks, M.A.W.; Holzäpfel, J.; Wenzel, T. Major, minor, and trace element composition of pyromorphite-group minerals as recorder of supergene weathering processes from the Schwarzwald mining district, SW Germany. *Am. Mineral.* **2014**, *99*, 1133–1146. [CrossRef]
50. Barkov, A.Y.; Nikiforov, A.A.; Barkova, L.P.; Martin, R.F. Occurrences of Pd–Pt Bismuthotellurides and a Phosphohedyphane-Like Phase in Sulfide Veins of the Monchepluton Layered Complex, Kola Peninsula, Russia. *Minerals* **2022**, *12*, 624. [CrossRef]

51. Fazle Bari, A.S.M.; Choppala, G.; Lamb, D.; Hamilton, J.L.; Sathish, C.; Rahman, M.M.; Naidu, R.; Aughterson, R.; Burton, E.D. Is beudantite a stable host phase of arsenic and lead? New insights from molecular-scale kinetic analyses. *J. Hazard. Mater.* **2024**, *480*, 136382. [CrossRef]
52. Takesue, M.; Hayashi, H.; Smith, R.L., Jr. Thermal and chemical methods for producing zinc silicate (willemite): A review. *Prog. Cryst. Growth Charact. Mater.* **2009**, *55*, 98–124. [CrossRef]
53. Fransolet, A.-M.; Bourguignon, P. Données nouvelles sur la fraipontite de Moresnet (Belgique). *Bull. Soc. Fr. Mineral. Cristallogr.* **1975**, *98*, 235–244. [CrossRef]
54. Foord, E.E.; Taggart, J.E.; Conklin, N.M. Cuprian fraipontite and sauconite from the Defiance-Silver Bill mines, Gleeson, Arizona. *Miner. Rec.* **1983**, *14*, 131–132.
55. Will, P.; Friedrich, F.; Grathoff, G.; Hochleitner, R.; Albert Gilg, H. Fraipontite/sauconite—A new interstratified clay mineral from the oxidation zone of the Zn-Pb-deposit Preguiça, Southern Portugal. In Proceedings of the Euroclay 2015, Edinburgh, UK, 5–10 July 2015; p. 107.
56. de Oliveira, D.; Silva, T.P.; Morais, I.; Fernandes, J. Chemical and mineralogical characterization of waste from abandoned copper and manganese mines in the Iberian Pyrite Belt, Portugal: A first step towards the waste-to-value recycling process. *Minerals* **2025**, *15*, 58. [CrossRef]
57. Frahm, E. Protocols, pitfalls, and publishing for pXRF analyses: From "know how" to "best practices". *J. Archaeol. Sci. Rep.* **2024**, *60*, 104831. [CrossRef]
58. Hawthorne, F.C.; Faggiani, R. Refinement of the Structure of Descloizite. *Acta Cryst.* **1979**, *B35*, 717–720. [CrossRef]
59. Brough, C.; Bowell, R.J.; Larkin, J. The geology of Vanadium deposits. In *An Introduction to Vanadium*; Chapter 4; Bowell, R., Ed.; Nova Science Publishers, Inc.: Hauppauge, NY, USA, 2019; pp. 87–117.
60. Silin, I.; Hahn, K.M.; Gürsel, D.; Kremer, D.; Gronen, L.; Stopi'c, S.; Friedrich, B.; Wotruba, H. Mineral Processing and Metallurgical Treatment of Lead Vanadate Ores. *Minerals* **2020**, *10*, 197. [CrossRef]
61. Huang, J.-H.; Huang, F.; Evans, L.; Glasauer, S. Vanadium: Global (bio)geochemistry. *Chem. Geol.* **2015**, *417*, 68–89. [CrossRef]
62. Santoro, L.; Putzolu, F.; Mondillo, N.; Boni, M.; Herrington, R. Influence of Genetic Processes on Geochemistry of Fe-oxy-Hydroxides in Supergene Zn Non-Sulfide Deposits. *Minerals* **2020**, *10*, 602. [CrossRef]
63. Boyle, R.W.; Jonasson, I.R. The geochemistry of antimony and its use as an indicator element in geochemical prospecting. *J. Geochem. Explor.* **1984**, *20*, 223–302. [CrossRef]
64. Kanellopoulos, C.; Sboras, S.; Voudouris, P.; Soukis, K.; Moritz, R. Antimony's Significance as a Critical Metal: The Global Perspective and the Greek Deposits. *Minerals* **2024**, *14*, 121. [CrossRef]
65. Schwarz-Schampera, U. Antimony. In *Critical Metals Handbook*; Gunn, G., Ed.; Wiley and Sons: Hoboken, NJ, USA, 2014; pp. 70–98.